EFFECT OF NON-HYDROSTATIC STRESS ON KINETICS AND INTERFACIAL ROUGHNESS DURING SOLID PHASE EPITAXIAL GROWTH IN SI

William Barvosa-Carter and Michael J. Aziz
Division of Engineering and Applied Sciences, Harvard University, Cambridge, MA 02138

ABSTRACT

We report preliminary *in-situ* time-resolved measurements of the effect of uniaxial stress on solid phase epitaxial growth in pure Si (001) for the case of stress applied parallel to the amorphous-crystal interface. The growth rate is reduced by the application of uniaxial compression, in agreement with previous results. Additionally, the velocity continues to decrease with time. This is consistent with interfacial roughening during growth under stress, and is supported by both reflectivity measurements and cross-sectional TEM observations. We present a new kinetically-driven interfacial roughening mechanism which is consistent with our observations.

INTRODUCTION

There is increasing interest in the effects of non-hydrostatic stresses on condensed phase processes such as diffusion and crystal growth. The focus of most work has mainly been to understand and account for the effects of stress on the energetics, or driving forces, for these processes. Little has been done to account for stress effects on the mobilities of the interfaces or atomic species involved, largely due to the difficulties associated with separating mobilities from driving forces for a given kinetic process. This is particularly true for recent studies of the morphological stability of stressed solids.

For solid-phase epitaxial growth (SPEG) in Si, however, the driving force varies negligibly compared to the mobility over the entire range of temperature and pressure studied. By studying SPEG in Si, we can begin to understand the effect of stress on the mobilities of the interfaces involved in the growth, and also how stress-dependent mobilities can affect the morphological evolution of the interfaces. In addition, by studying SPEG in pure Si, we can further the understanding of SPEG in Si-Ge alloy layers where both composition and stress play a role in the morphological evolution of the growing interface, but are hard to separate.

To describe the effects of temperature and pressure on a kinetic process, we use transition state theory (TST). In TST, the rate of a process is exponentially affected by the application of pressure, characterized by the activation volume, ΔV^*:

$$\text{rate} \propto \exp\left[-\frac{p\Delta V^*}{kT} \right] \tag{1}$$

where k is Boltzmann's constant, T is temperature, p is pressure. For SPEG of (001) Si, Lu *et al.* [1] measured $\Delta V^* = -0.28\ \Omega$, where Ω is the atomic volume of silicon. ΔV^* is negative, indicating that pressure exponentially enhances the SPEG rate.

In contrast to the hydrostatic pressure result, it was found by Aziz *et al.* [2] that compressive stress applied in the plane of the amorphous-crystal interface acts to retard the SPEG rate. To describe their results, they extended TST to include the effects of non-hydrostatic stress. The growth rate is exponentially affected by the application of an arbitrary stress state, σ_{ij}:

$$\text{rate} \propto \exp\left[\frac{\sigma_{ij}\Delta V^*_{ij}}{kT} \right] \tag{2}$$

where the response of the rate to an applied stress is now characterized by the activation strain tensor ΔV^*_{ij}.

For SPEG of (001) oriented Si, symmetry dictates that the activation strain tensor can only have two independent components, ΔV^*_{11} (= ΔV^*_{22}) and ΔV^*_{33}. All other components are zero. Aziz, Sabin, and Lu used *ex-situ* measurements to obtain $\Delta V^*_{11} = +0.15\ \Omega$.

Here, we present *in-situ* optical measurements of ΔV^*_{11}. In particular, we are interested in

the time-dependence of ΔV^*_{11} and the morphological stability of the amorphous-crystal interface.

EXPERIMENT

Samples were produced in a fashion similar to those described previously [3]. A 1 mm thick double-side polished (100) wafer was amorphized on both sides using ion-implantation at liquid nitrogen temperature ($^{28}Si^+$, 60 keV, 1e15/cm^2, 15μa/cm^2, followed by 180 keV, 2e15/cm^2, 7.5 μa/cm^2) and then diced, either along or at 45° to [011] cleavage directions, into long rectangular bars, 1 mm by 6 mm, shown in Fig. 1. The long sides of the bars consisted of the implanted [001] surfaces and either [011] or [010] sides. The unpolished sides of the bars were polished to a final surface roughness below 1 micron. It was found that a better polish on all sides of the bars led to fewer visible signs of plastic flow after annealing under load, presumably due to a reduced density of dislocation nucleation sites. Lowering the anneal temperature was also effective in reducing plastic flow, and all samples were annealed at 520 °C.

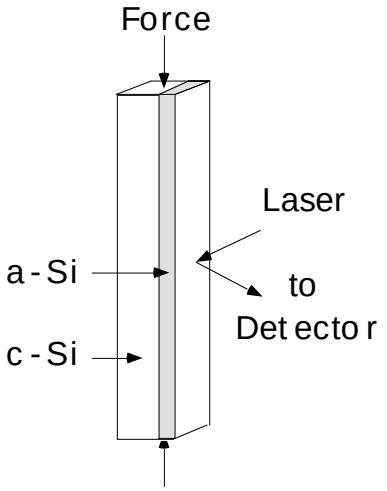

Figure 1. Sample geometry used in this work.

Amorphous layer thicknesses were determined using time-resolved reflectivity (TRR) [4]. The reflectivity of the sample varies as a function of amorphous layer thickness because of interference between reflections from the top surface of the sample and the buried amorphous-crystal interface. At the He-Ne wavelength of 632.5 nm and 520 °C, the reflectivity is modulated with a periodicity of 66.1 nm, which we assume to be independent of applied stress. By measuring reflectivity *vs.* time, we can deduce interface velocity *v* as a function of depth.

Fig. 2 shows the results of a typical experiment. Cracking limited the length of time each sample could be held under a given load, and load was applied for part of the regrowth only. This method allowed *v* before and after regrowth under load to be checked. The sample was initially held at minimal load. The load was then increased to -0.5 GPa, and reduced towards the end of the anneal, as shown in Fig. 2(a). The TRR obtained during this particular anneal is shown in Fig. 2(b). TRR data were then fit to a theoretical TRR trace and $v(t)$ was extracted. Temperature control in the loading furnace tended to cycle a few tenths of a degree, making it difficult to obtain low noise *in-situ* reflectivity. Thus, the $v(t)$ curves exhibit some variation. Additionally, when the load was changed on the sample, the reflected beam shifted position on the detector, making absolute reflectivity measurements impossible. In order to fit the resulting TRR curves, relative reflectivities for peaks and troughs were scaled to the theoretical values.

For all samples, we observed that *v* decreased upon the application of load, as is seen in Fig. 2(c). To characterize the change in *v* due to stress, the average velocity under load was compared with an extrapolation of the zero stress data. Averaging over all experiments gives a value of $\Delta V^*_{11} = +0.14 \pm 0.04\ \Omega$ which compares well with the results of Aziz *et.al.*

We also observed that *v* under load consistently continued to decrease with time. Due to the noise and temperature variations we could not easily quantify the rate of velocity decrease, but the sign of the rate of velocity change is significant. It is possible that this velocity change could be due to a changing stress in the amorphous layer. Such a time-evolving stress could explain our previous results on the effect of stress applied perpendicular to the growing interface [3]. In that experiment, we measured ΔV^*_{33} and found a smaller value than would be predicted by Eq. (2). However, based on the work of Witvrouw and Spaepen [5], we know that the stress in the amorphous layer will tend towards zero because the film can easily relax in the direction normal to the surface. Using their parameters for the temperature and time dependence of the viscosity of amorphous Si, we find that this relaxation should take place over a time scale on the order of the anneal time under load. If ΔV^*_{11} depends on the stress in the amorphous layer, then the stress effect should relax away. However, we observe a time-dependence in which the effect of applied stress becomes larger with time, not smaller. This suggests, then, that the stress state of the amorphous phase plays a minimal role in determining ΔV^*_{11} and likewise in determining ΔV^*_{ij} as a whole.

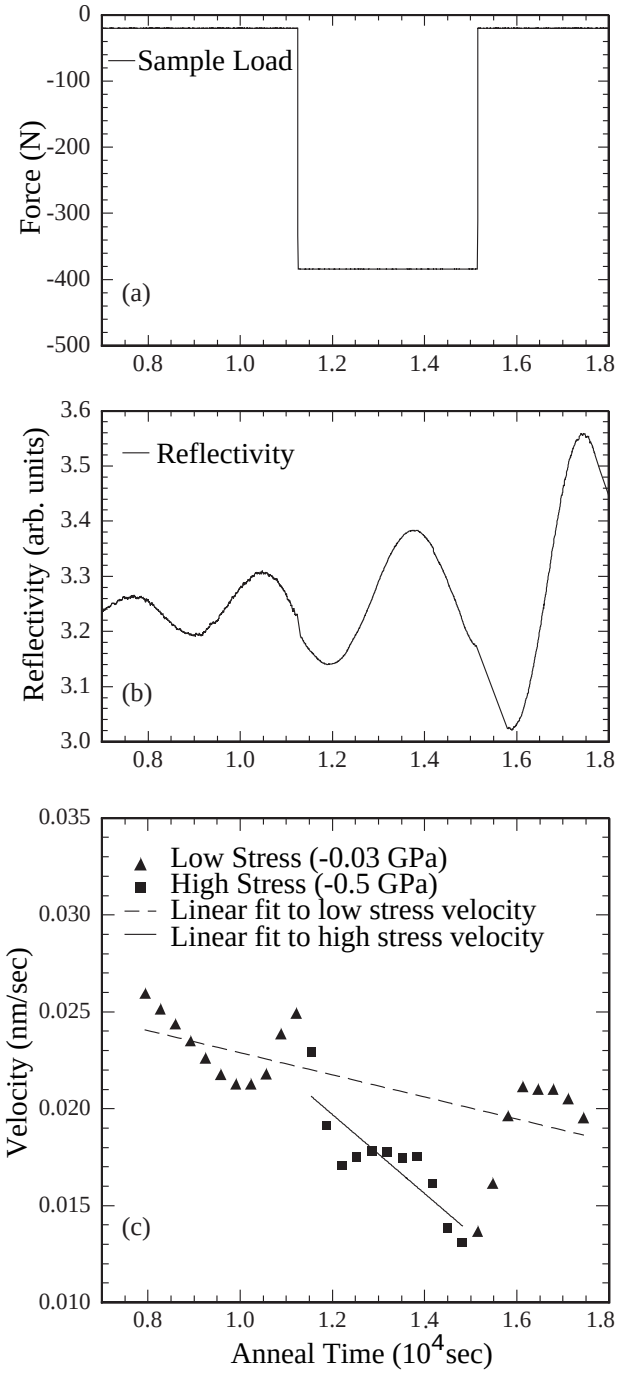

Figure 2. Response of SPEG rate to applied stress.

One explanation for the time dependence of ΔV^*_{11} is interfacial roughening. Both increasing stress concentrations and interface orientation deviations caused by the increasing roughness should cause *v* to be reduced. In an early experiment [6], we observed interfacial roughening in a sample regrown about 220 nm while being held under a very non-uniform stress of $\sigma_{33} \approx -0.5$ GPa. A cross-sectional TEM micrograph of this sample is shown in Fig. 3. We have subsequently observed similar roughening (though of a much smaller amplitude) in a cross-section of the ΔV^*_{11} sample from Fig. 2, which was quenched well after the stress was removed, possibly permitting the roughness to partially "heal". Additionally, increasing roughness causes a coincident damping of the TRR oscillations [7]. For a few samples which could be annealed under stress for long enough to establish relative maximum and minimum reflectivity values, there are indications of damping**.** In general, however, we are not able to quantify this effect.

DISCUSSION

We present two possible mechanisms for this roughening. The first is a thermodynamic instability mechanism which has been described previously [8]. In this mechanism, for any solid/fluid surface or interface under stress it is energetically favorable for the surface to undergo a morphological instability, and for spontaneous roughening to occur. The total energy of the system is reduced as strain energy is released at the peaks of the roughness at the cost of added interfacial energy. The balance of the strain and interfacial energies sets the length scale for the roughness. Assuming total strain relaxation for each peak and an interfacial energy, γ, equal to 1.0 J/m^2 [9], such an energy balance gives a spatial scale for break-even of roughly 400 nm, which is close to what we have observed. Note that this energetically-driven instability predicts that the interface is unstable both in compression and tension.

The second mechanism, illustrated in Fig. 4, is kinetically driven. For an amorphous-crystal interface under compressive stress, a stress concentration will develop in the valleys of the roughness relative to the peaks, as long as the stress in the amorphous relaxes. Because our measurement of a positive ΔV^*_{11} indicates that increasing compressive stress reduces *v*, the valleys should slow down relative to the peaks, and the roughness should generally increase. This kinetically-driven instability mechanism is different from the energetically-driven instability in several ways. (1) It is the effect of stress on the *interfacial mobilities* which is primarily responsible for the roughening. (2) While the energetically-driven instability can generally be suppressed under certain conditions (e.g. high

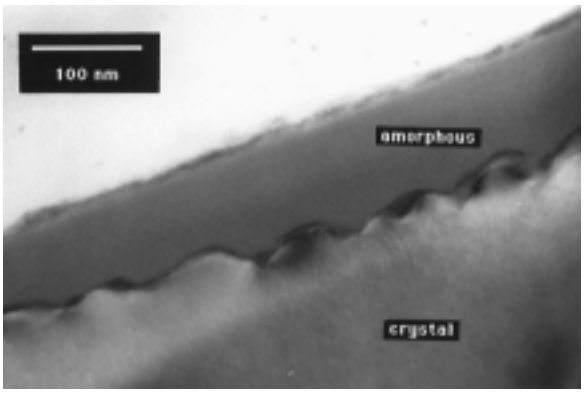

Figure 3. Amorphous-crystal interface for a sample grown 220 nm under a non-uniform stress of -0.5 GPa.

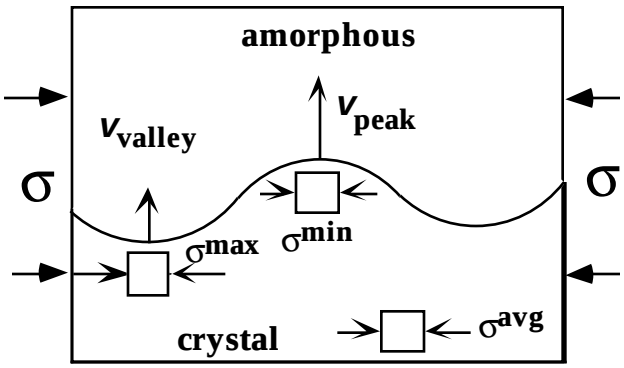

Figure 4. Proposed kinetically driven interfacial roughening mechanism

growth rate) this new kinetic instability does not appear to be suppressible. (3) The predicted stability of the interface changes with the sign of the stress: while the interface is unstable in compression, it is *stable* in tension.

We now present preliminary modeling of the time evolution of the roughness of the interface using this kinetic instability mechanism. We use the stress states calculated by Chiu and Gao [10] for a solid under stress whose surface is described by a cycloid of revolution. For small amplitudes, their solution approximates that for a sinusoidal surface perturbation, while for large amplitudes the solution is exact for a cycloid rough surface. As a function of amplitude A and wavelength λ, the in-plane stress at the trough and peak of the perturbation is given by:

$$\sigma_{11}^{peak} = \sigma_{11}^{ave} \frac{(1-kA)}{(1+kA)} \tag{3a}$$

$$\sigma_{11}^{trough} = \sigma_{11}^{ave} \frac{(1+kA)}{(1-kA)} \tag{3b}$$

where $k=2\pi/\lambda$. The choice of a cycloid to describe the interface between the amorphous and crystal phase is not crucial, it is used only to illustrate the essential features of this instability.

Given the local stress and curvature of the interface, within our kinetic instability model the growth rate of the interface is given by:

$$v = v_0 \exp\left[\frac{\Delta E^* + \sigma_{11} \Delta V_{ij}^*}{kT} \right] \{DF\} \tag{4}$$

Where ΔE* is the activation energy for growth, v_0 is the prefactor, and DF is a term that quantifies changes in the rate due to changes in the driving force. Generally, DF is a function of the free energy change upon transformation from amorphous to crystal, given by:

$$\Delta G = \Delta H - T\Delta S + \kappa\gamma\Omega \tag{5}$$

where ΔH and ΔS are the changes in enthalpy and entropy upon transformation, κ is the local interface curvature, γ is the interfacial energy, and Ω is the atomic volume.

The proper functional dependence of DF upon ΔG, however, is unknown for large ΔG/kT. Among the choices are:

(A): DF=constant;

(B): DF=[1–exp(ΔG/kT)];

(C): DF=sinh(ΔG/2kT).

Case (A) represents a situation of extreme non-equilibrium in which changes in the driving force have negligible effect on the rate. Case (B) is most commonly used in the study of phase transformations. Case (C) is also used occasionally. However, using the value for ΔG obtained

by Donovan *et. al.* [11], Eq. (4) can be well fit using all three forms for DF(ΔG) to Olson and Roth's SPEG rate data [4] (measured over ten decades in growth rate) by simply adjusting v_0 and ΔE*. Hence, no one functional form for DF(ΔG) can be ruled out, and we consider all three in our analysis.

Fig. 5 shows the growth rate for both peak and trough of a perturbation, using Eqs. (3) and (4), a peak to trough distance of 20 nm (A=10 nm), and the three choices DF including the effects of interface curvature at peak and trough. For forms (A) and (B) of DF(ΔG), the roughening rate, defined here by the difference in the peak and trough velocities, is monotonically increasing, indicating that shorter wavelengths should generally roughen faster. However, for form (C) for DF(ΔG), there is a wavelength that exhibits a maximal roughening rate. Although not plotted, this wavelength increases with increasing amplitude. It is important to note that at the highest aspect ratio, the cycloid surface is becoming highly cusped, and the solution may not properly represent the actual interface geometry of a sample.

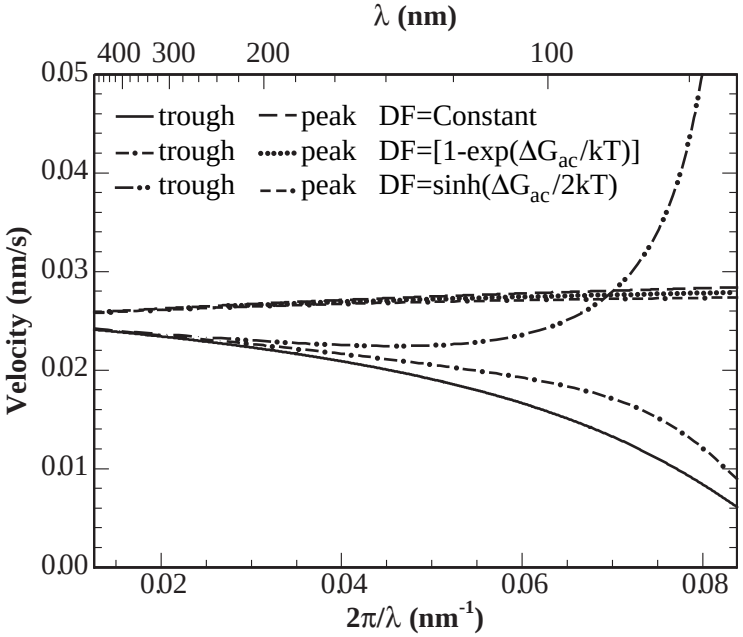

Figure 5. Growth rate at peak and trough vs. wavelength for a perturbation with A=10 nm.

We can make a simple iterative calculation of the evolution of the roughness of the interface at constant stress, as defined by the trough to peak height difference. The minimum possible roughness for the initial, un-stressed interface we take to be 0.5 nm, which is slightly smaller than that measured by Lohmeier *et.al.* [12] for a stress-free interface during SPEG in Si. The wavelength of the perturbation is fixed at λ=100 nm, which is the wavelength that we observed. Fig. 6 shows a plot of roughness *vs.* average distance regrown for the three choices for DF. For all three choices for DF(ΔG), the roughness of the interface increases nearly exponentially as a function of time. This is a natural consequence of the exponential change in the growth rate with increasing stress at the trough of the perturbation. Making the strong assumption that the micrograph in Fig. 3 represents what is going on in our uniformly stressed ΔV^*_{11} samples, we can make a preliminary and speculative quantitative comparison with the model to see whether all three forms for DF(ΔG) are consistent with our experiment. With this assumption, forms (A) or (B) for DF(ΔG) are consistent, but the roughness observed is much larger than that predicted using form (C). Fig. 7 shows the

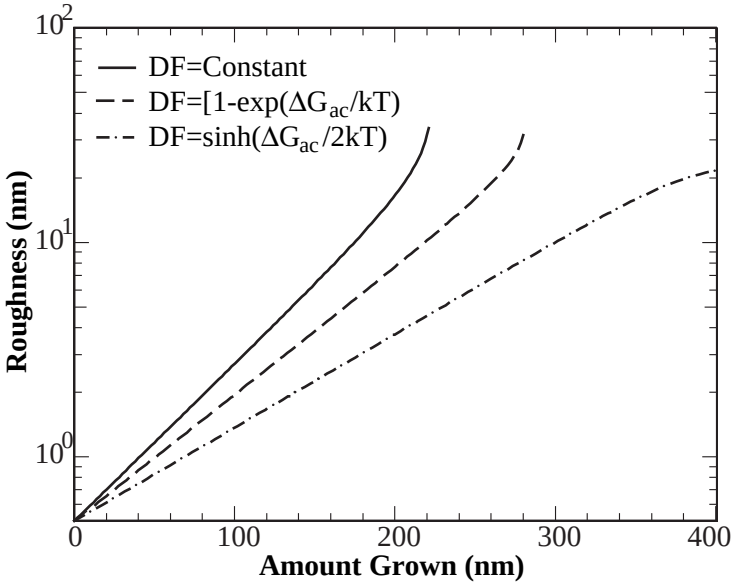

Figure 6. Roughness vs. distance regrown for the 3 forms for DF with an initial roughness of 0.5 nm.

result of a calculation of the roughness of the interface as a function of average distance regrown for initial roughnesses of 0.2, 0.5 and 1.0 nm and repeat lengths of λ=50nm, 100nm, 200nm, and 400 nm, assuming DF(ΔG) = constant.

The above kinetic instability analysis shows how roughness might evolve during SPEG under stress. However, many questions remain to be answered. For example, the mechanism by which the length scale of the roughening is chosen remains unclear. Within the kinetic model we present, the roughening rate is greater for smaller wavelengths. Additionally, for the case of a cycloid surface, the wavelength with maximum growth rate will change as a function of the amplitude of the perturbation. It is possible that changes in the driving force due to capillarity can counterbalance the stress effect at small wavelengths if we choose form (C). However, (C) predicts a roughening rate that may be too small.

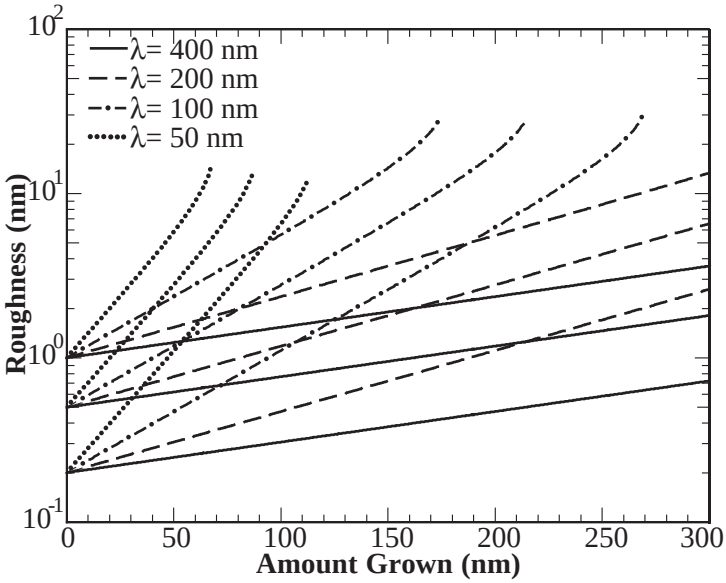

Figure 7. Roughness versus amount grown for different initial roughnesses and wavelengths

SUMMARY

We have used *in-situ* TRR to measure the effect of stress applied in the plane of the amorphous layer on the SPEG rate in Si. We find that the rate is reduced with stress, in agreement with previous measurements, and is characterized by $\Delta V^*_{11} = +0.14 \pm 0.04\ \Omega$. Additionally, the magnitude of the stress effect increases with time. This can be attributed to roughening of the interface during growth. A new kinetically-driven interfacial roughening mechanism is consistent with our observations.

ACKNOWLEDGMENTS

We thank J.C. McCallum for providing the program to calculate *v* from TRR data. This research was supported by NSF-DMR-95-26583 and subsequently by NSF-DMR-94-00396.

REFERENCES

[1] G.-Q. Lu, E. Nygren, and M.J. Aziz, J. Appl. Phys. **70**, 5323 (1991).
[2] M.J. Aziz, P.C. Sabin, and G.-Q. Lu, Phys. Rev. B **44**, 9812 (1991).
[3] W. B. Carter and M. J. Aziz, Mater. Res. Soc. Symp. Proc. **356**, 87 (1995).
[4] G.L. Olson and J.A. Roth, Mater. Sci. Rep. **3**,1 (1988).
[5] A. Witvrouw and F. Spaepen, J. Appl. Phys. **74**, 7154 (1993).
[6] M.J. Aziz, Mater. Res. Soc. Symp. Proc. **321**, 449 (1993).
[7] X. Zeng, T.-C. Lee, J. Silcox, and M.O. Thompson, Mater. Res. Soc. Symp. Proc. **321**, 503 (1994).
[8] R.J. Asaro and W.A. Tiller, Metall. Trans. **3**, 1789 (1972); M.A. Grinfeld, Sov. Phys. Dokl. **31**, 831 (1986); D.J. Srolovitz, Acta Metall. **37**, 621 (1989).
[9] F. Spaepen, Acta Metall. **26**, 1167 (1978).
[10] C.-H. Chiu and H. Gao, Int. J. Solids Struct. **30**, 2983 (1993).
[11] E. P. Donovan, F. Spaepen, D. Turnbull, J.M. Poate, and D.C. Jacobson, J. Appl. Phys. **57**, 1795 (1985).
[12] M. Lohmeier, S. DeVries, J.S. Custer, E. Vlieg, M.S. Finney, F. Priolo, and A. Battaglia, Appl. Phys. Lett. **64**,1803 (1994)